Electronic Supplementary Information

A Noble Metal Seed-Mediated Approach to General and Mild Synthesis of Non-noble Metal Nanoparticles Stabilized by A Metal-Organic Framework for Highly Efficient Catalysis

Yu-Zhen Chen,[a,‡] Linfeng Liang,[a,b,‡] Qihao Yang,[a] Maochun Hong,[b] Qiang Xu,[c] Shu-Hong Yu,[a] and Hai-Long Jiang[a,b],*

[a]*Hefei National Laboratory for Physical Sciences at the Microscale, Key Laboratory of Soft Matter Chemistry, Chinese Academy of Sciences, Collaborative Innovation Center of Suzhou Nano Science and Technology, Department of Chemistry, University of Science and Technology of China, Hefei, Anhui 230026, P.R. China*

[b]*State Key Laboratory of Structural Chemistry, Fujian Institute of Research on the Structure of Matter, Chinese Academy of Sciences, Fuzhou, Fujian 350002, P.R. China*

[c]*National Institute of Advanced Industrial Science and Technology (AIST), Ikeda, Osaka 563-8577, Japan*
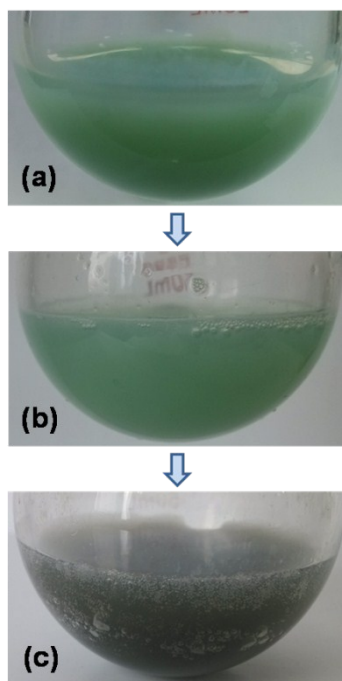
Fig. S1 As a representative, the synthesis progress for Ag-doped Ni/MIL-101 can be visibly monitored by the obvious color evolution in the solution: (a) The pale green Ag^+Ni^{2+}/MIL-101 aqueous solution before the reduction by NH_3BH_3; (b) the deep green aqueous solution obtained at the beginning of the hydrolysis of NH_3BH_3, in which only the Ag^+ was reduced to Ag NPs as seeds. The generated very few bubbles are due to the presence of tiny amount of Ag NPs; (c) then the color became darker and darker gradually within a few minutes during the hydrogen generation and reduction process, and the bubbles becomes more and bigger, revealing that the reduction of Ni^{2+} NPs to Ni NPs covered on the pre-formed Ag seeds, thus to afford Ag-doped Ni/MIL-101.
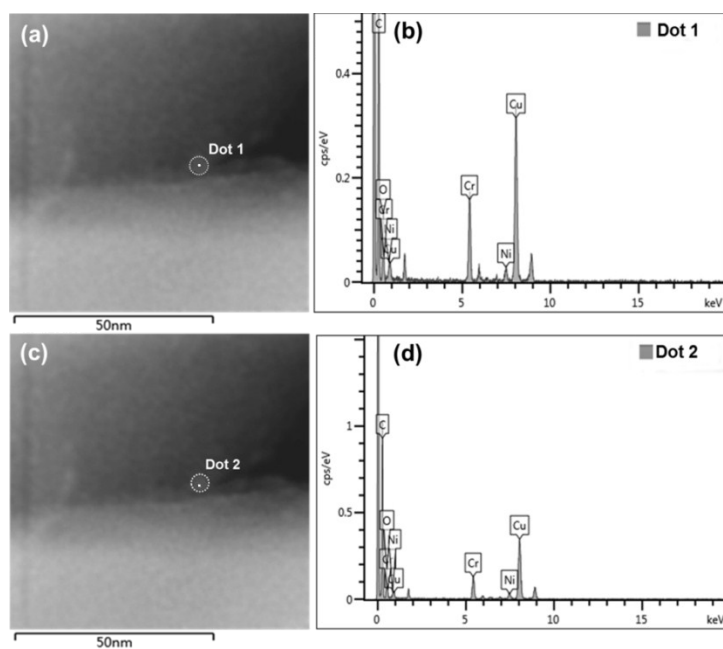
Fig. S2 (a, c) HAADF-STEM images and (b, d) the corresponding EDS spectra for as-synthesized Ag-doped Ni/MIL-101 sample. The point 1 in (a) and 2 in (c) lie in middle and edge of Ag-doped Ni NPs, respectively. The Cu and Cr signals originate from Cu grid and MIL-101 support, respectively. The EDS spectra for point 1 and 2 marked for Ag-doped Ni NPs only show the element Ni because the content of Ag is too low to be detectable.
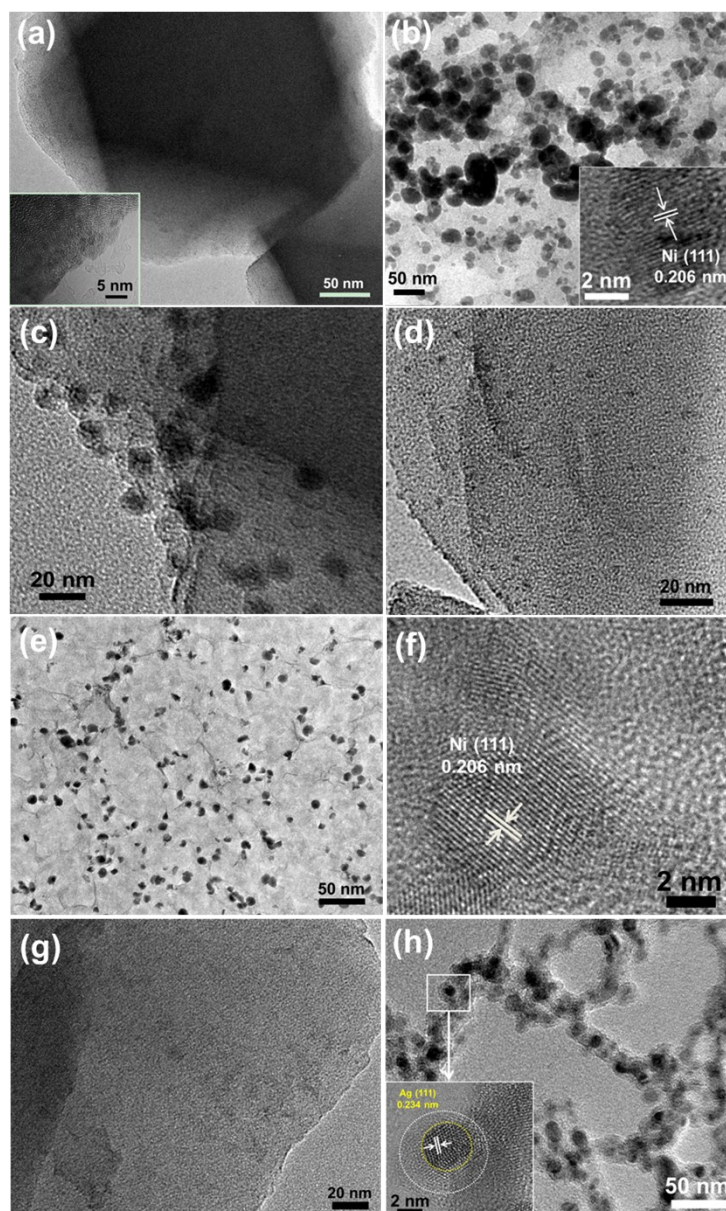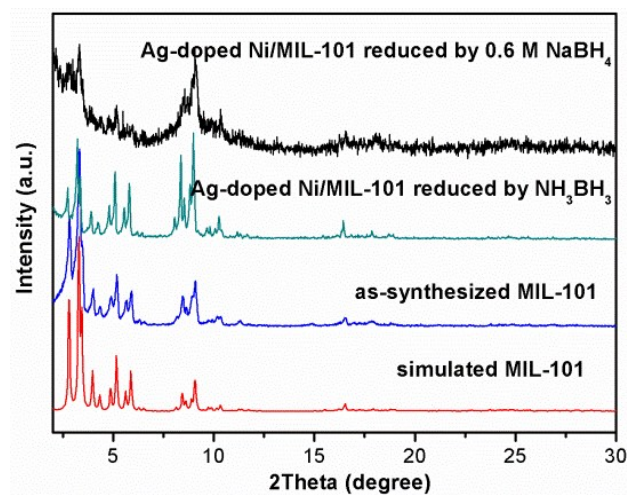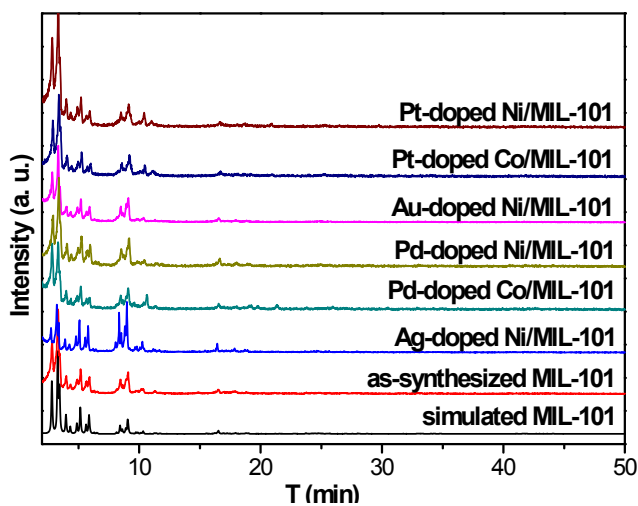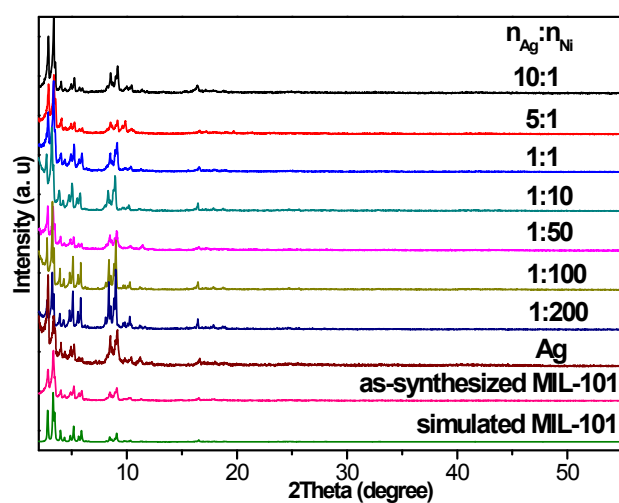
Fig. S3 TEM image of (a) Ag-doped Ni/MIL-101 (reduced by NH_3BH_3) with Ag/Ni molar ratio of 1/200, (b) PVP-stabilized Ni NPs (reduced by $NaBH_4$, inset: HRTEM image for Ni NP) (c) Ni/MIL-101 (reduced by $NaBH_4$), (d) Ag/MIL-101 (reduced by NH_3BH_3), and (e) pure Ag-doped Ni (1/200) NPs without stabilizer. (f) HRTEM image of pure Ag-doped Ni NP, in which the lattice fringes with 0.206 nm spacing are assigned to the (111) plane of the face-centered cubic (fcc) Ni. (g) Ni^{2+}/MIL-101 and (h) PVP-stabilized Ag@Ni core-shell NPs (reduced by NH_3BH_3) with Ag/Ni molar ratio of 1/1 (inset: HRTEM image for Ag@Ni NP).

(a)

(b)

(c)

Fig. S4 PXRD patterns of (a) Ag-doped Ni/MIL-101 reduced by 0.6 M NaBH$_4$ or

NH$_3$BH$_3$ aqueous solution, (b) simulated MIL-101, as-synthesized MIL-101, Ag-doped Ni/MIL-101, Pd-doped Co/MIL-101, Pd-doped Ni/MIL-101, Pt-doped Ni/MIL-101, Pt-doped Co/MIL-101 and Au-doped Ni/MIL-101 with noble/non-noble metal molar ratio from 1/100 to 1/200, and (c) simulated MIL-101, as-synthesized MIL-101, Ag/MIL-101, and Ag-doped Ni/MIL-101 with various molar ratios of Ag and Ni.
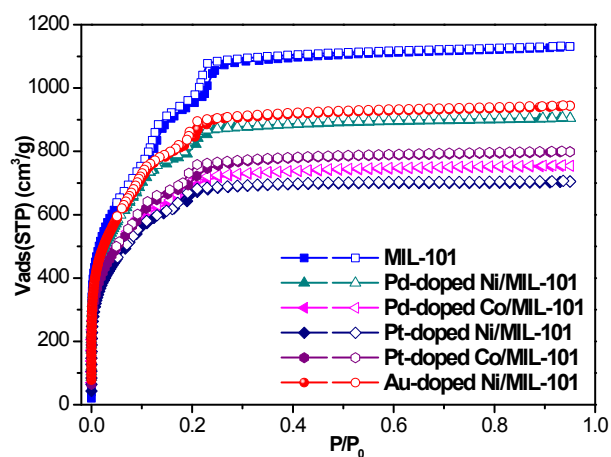
(a)
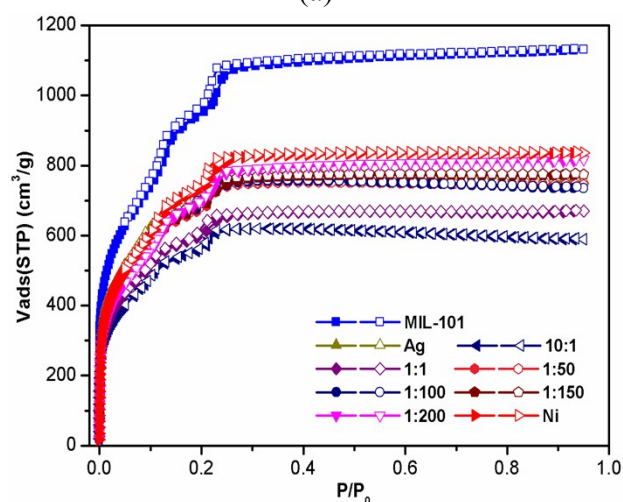
(b)

Fig. S5 N_2 sorption isotherms of (a) as-synthesized MIL-101, Pd-doped Co/MIL-101, Pd-doped Ni/MIL-101, Pt-doped Ni/MIL-101, Pt-doped Co/MIL-101 and Au-doped Ni/MIL-101 with the corresponding surface areas of 3660, 2347, 2711, 2250, 2328, 2941 m^2/g, respectively. (b) N_2 sorption isotherms of as-synthesized MIL-101, Ag/MIL-101and Ag-doped Ni/MIL-101 with Ag/Ni molar ratios of 10/1, 1/1, 1/5, 1/50, 1/100 and 1/200 at 77 K, with the corresponding surface areas of 3660, 2456, 2034, 2142, 2452, 2453, 2490, 2460, 2753 m^2/g, respectively. Filled and open symbols represent adsorption and desorption branches, respectively.
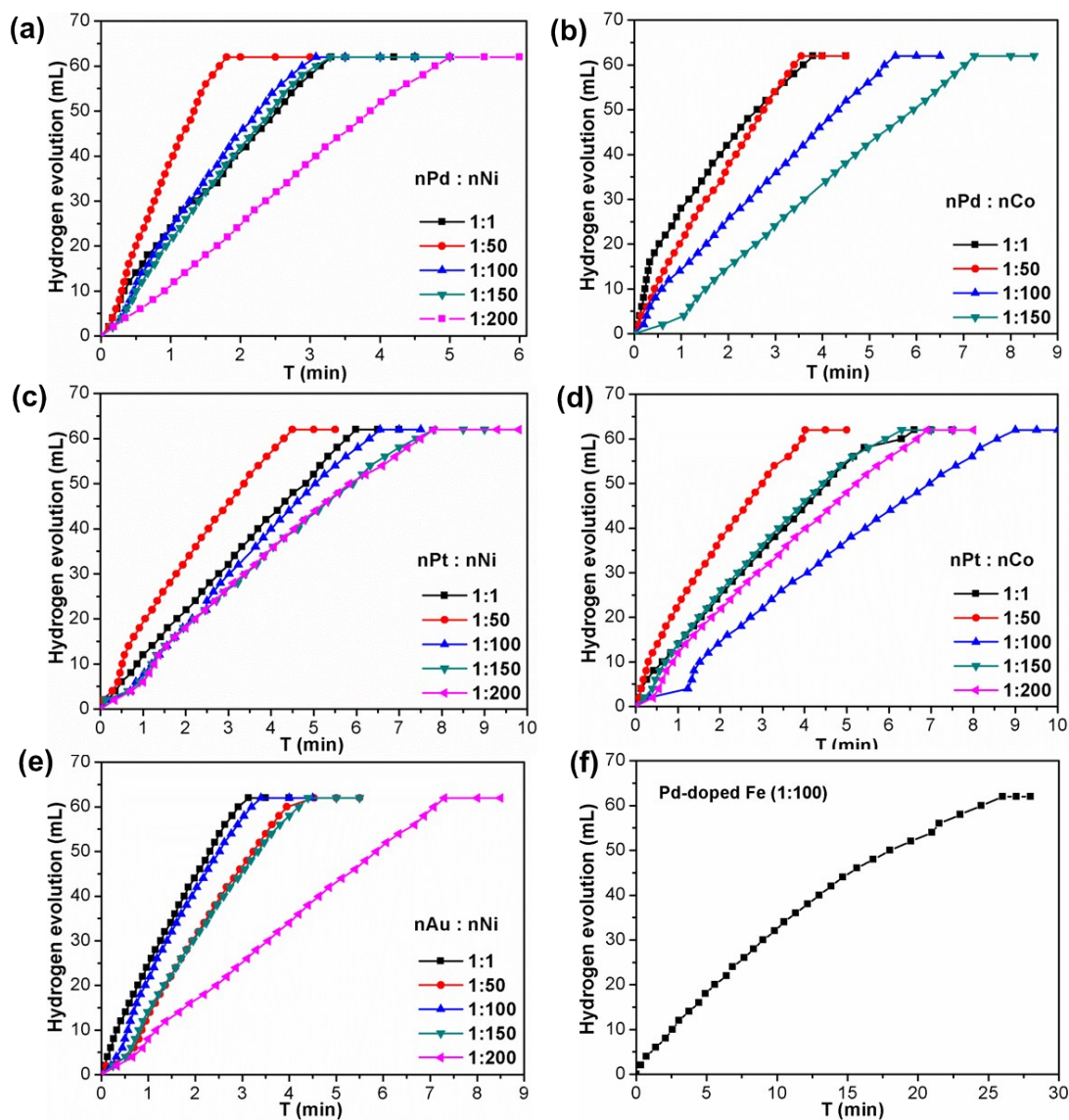
Fig. S6 Plots of time *vs* volume of hydrogen generated from the catalytic hydrolysis of NH₃BH₃ over (a) Pd-doped Ni/MIL-101, (b) Pd-doped Co/MIL-101, (c) Pt-doped Ni/MIL-101, (d) Pt-doped Co/MIL-101, (e) Au-doped Ni/MIL-101 catalysts with different noble/non-noble metals molar ratios, and (f) Pd-doped Fe/MIL-101 (1:100) at 25 °C. The Fe species has inferior activity compared to Ni and Co. Therefore, only catalytic study over Pd-doped Fe/MIL-101 (1:100) was conducted.

Table S1. Catalytic reaction rate constant k and TOF value of Ag-doped Ni/MIL-101 catalysts with different Ag/Ni ratios for hydrolytic dehydrogenation of NH_3BH_3 (TOF = $k/(V_0 \cdot n_{metal})$, V_0 = 24 L/mol, T= 25 °C).

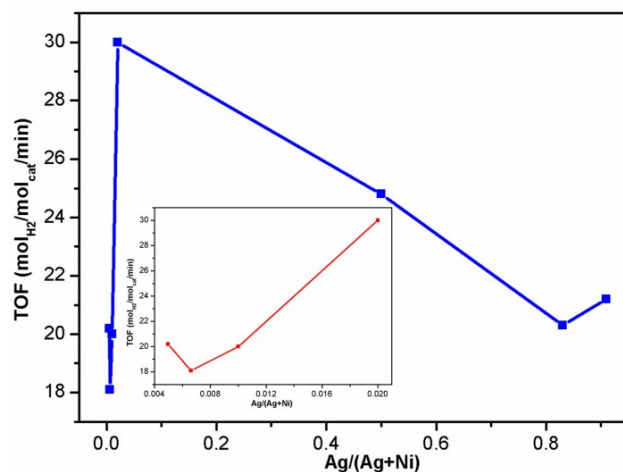| n_{Ag}: n_{Ni} (mol:mol)	K ($mL_{H2} \cdot min^{-1}$)	TOF ($mol_{H2} \cdot mol_{metal}^{-1} \cdot min^{-1}$)
10:1	7.31	21.2
5:1	8.94	20.3
1:1	7.62	24.8
1:50	10.8	30
1:100	7.21	20
1:150	6.51	18.1
1:200	7.28	20.2

Fig. S7 Plots of TOF value of hydrogen release versus Ag-doped Ni/MIL-101 catalysts with various Ag/(Ag+Ni) molar ratios. Reaction conditions: 0.875 mmol ammonia borane, 20 mL H_2O, (Ag+Ni)/NH_3BH_3 = 0.017 in molar ratio for all catalysts.
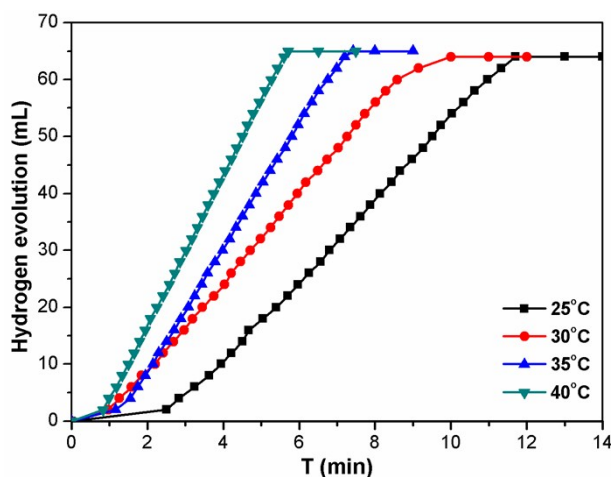

Fig. S8 Plots of time versus the volume of hydrogen generated from the hydrolysis of ammonia borane catalyzed by the Ag-doped Ni/MIL-101 catalyst with Ag/Ni atomic ratio of 1/200 at different temperatures. It can be seen that the lower the reaction temperature, the longer the initiation period. After the initiation process, a rapid and almost linear hydrogen evolution can be observed.
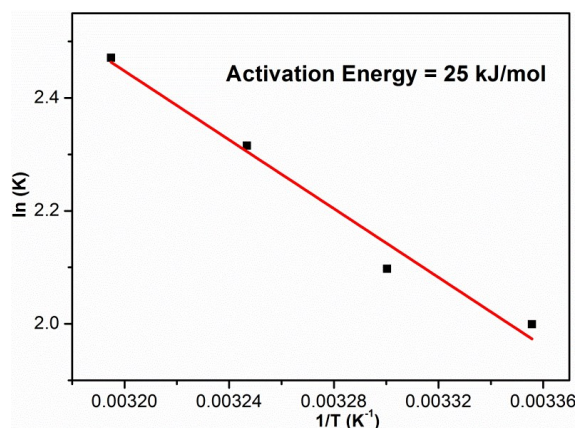
Fig. S9 Plots of ln (K) versus 1/T of hydrogen generated from ammonia borane (0.875 mmol, 20 ml) in the presence of Ag-doped Ni/MIL-101 catalyst with Ag/Ni molar ratio of 1/200 ((Ag+Ni)/NH_3BH_3 = 0.017 in molar ratio) at 25, 30, 35 and 40 °C and the calculated activation energy is 25 kJ/mol.
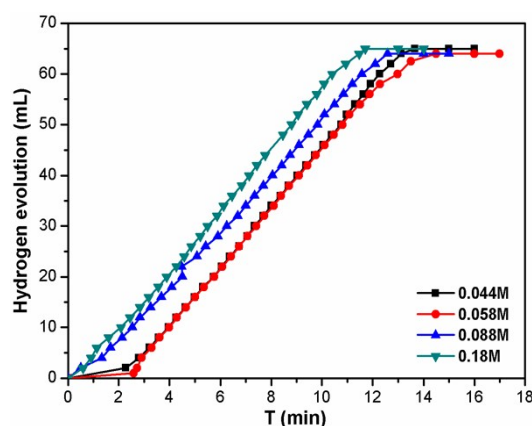
Fig. S10 Plots of time versus the volume of hydrogen generated from the hydrolysis of ammonia borane over Ag-doped Ni/MIL-101 catalyst with Ag/Ni molar ratio of 1/200 at different concentrations of ammonia borane ([NH_3BH_3] = 0.875 mmol, T = 25 °C), indicating that the catalytic hydrolysis of ammonia borane is of zero order with respect to the substrate concentration. It can be seen that the initiation process is dependent on the NH_3BH_3 concentration while other reaction conditions are fixed. The higher NH_3BH_3 concentration is, the shorter initiation period.

S11

Table S2. Performance comparison of Ag-doped Ni/MIL-101 catalyst with various catalysts.

Catalyst	Ea kJ·mol^{-1}	TOF (mol$_{H2}$·mol$_{metal}$$^{-1}$·min^{-1})	Ref.
Ag-doped Ni/MIL-101 (Ag/Ni molar ratio = 1/200)	25	20.2	This work
PSMA-Ni	38.12	10.1	1
zeolite confined palladium (0)	56	5.6	2
Ni/SiO$_2$	34	13.2	3
Ag-Ni/C	52	-	4
Ni$_{0.97}$-Pt$_{0.03}$	57	-	5
VP stabilized Au@Co core-shell	-	13.6	6
CVD-Ni/ZIF-8	-	14.2	7
Ni/γ-Al$_2$O$_3$	-	1.7	8
Pt/Al$_2$O$_3$	21	-	9
Ag@CoNi/graphene	47	-	10

Table S3. Inductively coupled plasma atomic emission spectrometry (ICP-AES) analysis results for catalysts. The results have confirmed that the actual ratios of noble/non-noble metals are very close to the nominal values.

Nanoparticles	Metal content (%)	n_{noble} / $n_{non\text{-}noble}$ (mol / mol)	
		Actual value	Nominal value
Ag-doped Ni	1.81	1/167	1/200
Pd-doped Ni	1.51	1/210	1/200
Pd-doped Co	1.75	1/144	1/150
Pt-doped Ni	1.43	1/85	1/100
Pt-doped Co	1.73	1/96	1/100
Au-doped Ni	1.63	1/88	1/100

Experimental process for ICP characterization: First, the instrument was preheated for about 30 min. Second, sample treatment: 10 mg of sample was dissolved in 3 mL concentrated HNO_3 followed by heating to 80 °C to remove organics. The residue was dissolved with 1 mL HNO_3 and some water, and then continuously adding water to make solution volume to 10 mL (a constant volume). Third, work curve was made and the metal ions in solution were measured.
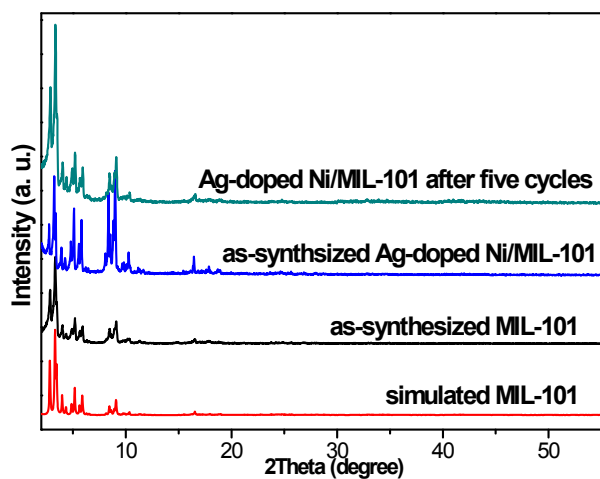
Fig. S11 PXRD patterns for Ag-doped Ni/MIL-101 catalyst with Ag/Ni molar ratio of 1/200 and the catalyst after 5 cycles of NH_3BH_3 hydrolysis, revealing the well-retained crystallinity and framework structure of MIL-101, and also the absence of aggregation of tiny Ag-doped Ni NPs in both catalysts before and after five runs of recycling experiments.

References

1. Ö. Metin and S. Özkar, *Int. J. Hydrogen Energy*, 2011, **36**, 1424-1432.

2. M. Rakap and S. Özkar, *Int. J. Hydrogen Energy*, 2010, **35**, 1305-1312.

3. Ö. Metin, S. Özkar and S. Sun, *Nano Res.*, 2010, **3**, 676-684.

4. F. C. Yao, L. Zhuang, Y. L. Cao, X. P. Ai and H. X. Yang, *Int. J. Hydrogen Energy*, 2008, **33**, 2462-2467.

5. F. Cheng, H. Ma, Y. Li and J. Chen, *Inorg. Chem.*, 2007, **46**, 788-794.

6. J.-M. Yan, X.-B. Zhang, T. Akita, M. Haruta and Q. Xu, *J. Am. Chem. Soc.*, 2010, **132**, 5326-5327.

7. P. Z. Li, K. Aranishi and Q. Xu, *Chem. Commum.*, 2012, **48**, 3173-3175.

8. M. Chandra and Q. Xu, *J. Power Sources*, 2006, **156**, 190-202.

9. M. Chandra and Q. Xu, *J. Power Sources*, 2007, **168**, 135-142.

10. L. Yang, J. Su, X. Meng, W. Luo and G. Cheng, *J. Mater Chem A*, 2013, **1**, 10016-10023.